1st TMS/ABM International Materials Congress
TMS CO-ORGANIZADOR
ANAIS PROCEEDINGS
ISSN 1516-392X

POROSITY AND SURFACE TOPOGRAPHY CHARACTERIZATION OF TITANIUM SAMPLES[1]

Alexandre Antunes Ribeiro[2]
Anderson Camargo Moreira[3]
Celso Peres Fernandes[4]
Luiz Carlos Pereira[5]
Marize Varella de Oliveira[6]

Abstract
Porous titanium allows bone formation and bone ingrowth in vivo providing a better implant fixation of surgical implants. Some important parameters of porous biomaterials are porosity, pore size, pore shape and pore homogeneity as they influence mechanical properties and biocompatibility. Many techniques have been used to characterize these parameters and different kinds of information can be achieved depending on the method used. Porous titanium samples were manufactured in this work by powder metallurgy, using pure titanium powders mixed with a pore former additive. The porosity quantification was assessed by geometric method, gamma-ray transmission technique, quantitative metallographic analysis and computed x-ray microtomography. Qualitative evaluation of pore morphology and surface topography were performed by optical microscopy, scanning electron microscopy and confocal scanning optical microscopy. The results allowed the comparison of the different techniques and the determination of the advantages and difficulties of each one, according to the samples studied.

Key words: titanium; porosity; topography.

[1] 1st TMS/ABM.
[2] D.Sc. (LATEP/DPCM/Instituto Nacional de Tecnologia).
[3] Dr. Eng. student (LMPT/PGMAT-EMC/Universidade Federal de Santa Catarina).
[4] Dr. Eng. (LMPT/EMC/Universidade Federal de Santa Catarina).
[5] D.Sc. (PEMM/COPPE/Universidade Federal do Rio de Janeiro).
[6] D.Sc. (LATEP/DPCM/Instituto Nacional de Tecnologia).

INTRODUCTION

Porous metallic biomaterials represent superior alternatives to traditional non-porous metallic implants for two main reasons. First, open porosity can enhance bone ingrowth improving fixation at the interface between bone and implant. Second, porosity decreases the mismatch in stiffness between bone and implant, thus reducing stress-shielding effects which shorten the implant lifetime through bone resorption and loosing. The major benefits of porous Ti and Ti alloys, compared with other bone graft materials, include their good mechanical strength an elastic modulus close to the bone and porous structure, providing biological fixation, and good biocompatibility[1,2].

The influence of pore volume fraction, pore size, pore spatial distribution and morphology on the mechanical and biological properties of the porous biomaterials is critical to optimize the manufacturing processing parameters. These porosity parameters must be carefully controlled, since bone ingrowth requires interconnected pores, pore sizes in the range of 100–500 μm and porosity quantity in the range of 40–90%. Micropores (< 20 μm) and nanopores (1–10 nm) also contribute to higher bone protein adsorption, which favors cellular adhesion and implant osseointegration. In addition, a high pore wall roughness may encourage intimate contact between bone and implant[3-6].

A number of approaches to the fabrication of porous Ti and Ti alloys have been reported, including sintering loose Ti powder or fiber, slurry sintering, rapid prototype, reactive sintering, hollow sphere sintering and gas entrapped techniques[1]. Powder metallurgy (PM) is an advantageous process as all steps are performed in the solid state, avoiding the high reactivity of Ti in the molten state. Another benefit is the possibility of obtaining an adjustable porosity amount, pore shape, and pore size distribution, by using a pore former additive. Pores can be originated from the particle compacting arrangement or changes in this arrangement, when pore former particles are used and their decomposition increases porosity. Solid-state diffusion in the sintering step also can generate pores[7,8].

Both the porosity and surface topography of biomaterials must be adequately characterized, since this provides baseline information upon which their performance can be related. Many techniques have been used to analyze these parameters and different kinds of information can be achieved depending on the method used. The aim of the present work was to study the porosity and surface features of the porous titanium samples processed by powder metallurgy. The evaluation was performed by different porosity methods and surface topography analyses. The results allowed the comparison of the different techniques and the determination of the advantages and difficulties of each one, according to the porous titanium samples studied.

MATERIALS AND METHODS

Pure Ti powder grade 2 (Micron Metals-EUA) made by HDH (hydrogenation-dehydrogenation) process, with acicular shape, particle size range of 149-177 μm and an organic additive (urea), as pore former, were used to make the samples by a powder metallurgy route. Cylindrical samples with 5.4 mm/height and 8.4 mm/diameter, composed by 85% wt-Ti/15% wt mixed with -urea (149-177 μm particle

size range) was compacted by cold isostatic pressing at 300 MPa. The samples were treated at 200ºC/2h to eliminate the organic additive and sintered at 1200ºC/2h in vacuum furnace (~10^{-6} Torr).

The total porosity (P), obtained by the geometric method (GM) was determined by P = 100 – RD, being RD the relative density, which is determined dividing the geometric density (mass/volume) by the absolute Ti density (4.5 g/cm^3). About 8 measurements were performed in the GM method.

The gamma-ray transmission (GRT) technique consists in the attenuation that an incident radiation beam undergoes when go across this material. The Beer's law establishes the relationship between the attenuated radiation intensity by a sample and other parameters of the system. The experimental setup is constituted by a micrometer automated table for the sample positioning, Am-241 radioactive source (59.53 keV, 100 mCi), 2 mm diameter Pb collimators, NaI(Tl) detector and appropriate nuclear electronics. The linear attenuation coefficient of the porous sample was obtained by beam transmission at 26 random points along the sample with 600s measurement time. The porosity determination of the sample, in relation to his linear attenuation coefficient, is done by the following equation:

$$\phi = 100\left(\frac{\mu_p - \mu_s}{\mu_p}\right)$$

where ϕ is the porosity, μ_p is the linear attenuation coefficient the sample totally solid (same material of the sample but without pores) and μ_s is the linear attenuation coefficient for the porous sample, both in cm^{-1}.

The mass attenuation coefficient can be written as:

$$\mu' = \mu / \rho$$

where μ' is the mass attenuation coefficient (cm^2 g^{-1}), and ρ is the density of the sample (g cm^{-3})[9].

Calculations of the mass attenuation coefficients of the samples were carried out by the WinXCOM program. The software can generate cross sections and attenuation coefficients for elements, compounds or mixtures in the energy range between 1 keV and 100 GeV, in the form of total cross sections and attenuation coefficients as well as partial cross sections of the following processes: incoherent scattering, coherent scattering, photoelectric absorption and pair production in the field of the atomic nucleus and in the field of the atomic electrons[10-12].

A sample transverse section was prepared for optical microscopy using the standard methodology. Porosity volume fraction, pore size distribution and average autocorrelation function C(u) were determined by quantitative metallographic analysis (QMA), using Imago software, in about 10 random images. The Imago software is a program with tools to estimate geometrical and topological parameters of porous medium in 2D images obtained by optical microscopy or scanning electron

microscopy. While the porosity is related to the probability of an arbitrary pixel of the image to belong to the pore phase, the average autocorrelation function, C(u), relates to the probability of finding two pixels separated by (u) and belonging to the pore phase. These relations constitute the first and second order statistics (or moments) of the image[13-14]. The average autocorrelation function C(u) was determined with goal to generate 3D models of the sample in order to determine the porosity and the pore size distribution based on 3D volume. The images presented noise interferences and illumination gradients; because of this they underwent cuts to choose the region of interest and were submitted to filter treatment in order to eliminate these interferences.

The computed x-ray microtomography (μ-CT) is an accurate non-destructive technique. The system used was a SKYSCAN 1172 scanner consisting of an X ray tube (20-100kV, 0-250μA), a 10Mpixel CCD detector and system for sample and detector movement. The tomography measurements were accomplished with the following scan conditions: 100 kV, 100 μA, no filter, 2 frames averaged, 2655 ms integration time per frame, 360.0° total rotation a ngle with 0.25° step size of rotation angle. The equipment reaches ~0.8μm image resolution. To make examinations, x-rays are directed from a high-power source toward the sample, and a detector on the opposite side of the sample measures the intensity of the transmitted x-rays. A two-dimensional “projection” image is produced by accurately rastering the x-ray beam across the sample. Then the sample is carefully moved (usually rotated around 360°) relative to the x-ray beam and the process is repeated to produce additional two-dimensional images from various view points. Using a sophisticated Fourier transform algorithm, the two-dimensional images then are combined to generate a complete three-dimensional map of the sample. In the common case of x-ray absorption tomography, the inner structure of the object under study is represented by the linear attenuation coefficient, which can be assumed to be proportional to the mass density.

Pore morphology and surface topography were evaluated by optical microscopy (OM), scanning electron microscopy (SEM) conducted in a JEOL JSM-6460LV, operating at 20kV and confocal scanning optical microscopy (CSOM) Alicona InfiniteFocus®. CSOM and OM techniques have the unique capability of creating a bright image of the in-focus region of the specimen while causing all out-of-focus regions to appear dark. One of the major limitations of OM is an inherent narrow depth of field. However, by using a confocal microscope to assemble a series of optical sections, each taken at a different focal plane, a “through-focus” image can be created which has “infinite” depth of field. This ability to overcome the limitation of a narrow depth of field has allowed the CSOM to find a unique role in imaging non-flat or translucent specimens[15]. Through the construction of an optical image of a rough surface, CSOM also has the ability to create topographic maps. The topographic map is a digital image in which each pixel is assigned a value that represents the *z*-level. Each pixel may be thought of as an *x-y-z* coordinate in the 3D surface. The actual surface area of the specimen can be estimated by geometric construction of the surface represented by topographic map. Once the surface area is computed, roughness and waviness of the surface can be characterized[16].

RESULTS AND DISCUSSION

Figure 1a shows the SEM topographic and figure 1b shows the optical micrograph views from the Ti porous sample, which porous microstructure consists of closed micropores less than 50 μm and large interconnected macropores in the range of 100–500 μm. Table 1 presents the porosity values from the sample, obtained by the four techniques employed in this work. According to the porosity results (Table 1) and pore morphology (Figures 1a, 1b), the sample presents adequate porosity for bioengineering applications[6]. The GM and GRT techniques show similar porosity levels (Table 1) in comparison with μ-CT values. On the other hand, the values measured by QMA are substantially higher than those obtained from GM, GRT and μ-CT. Also the standard deviation values of the GM and QMA measurements are higher (GM/2.80; QMA/3.00) than those obtained by the other two techniques (GRT/1.14; μ-CT/0.55).

Figure 2 presents the frequency of pores of the Ti porous sample as a function of pore size range for 2D image (Figure 1b) obtained by quantitative metallographic analysis technique. The pore size distribution range determined is 8.81-58.74 μm in radius. The frequency of pores related to this distribution range is 67.32%.

The Ti porous sample presented agreement between 2D and 3D average autocorrelation functions C(u), indicating that the generated model can represent the sample. Figure 3a shows the 2D binary section generated by model of the sample, where pore is the white phase. Figure 3b presents the 3D model created by truncated Gaussian method[13], which constructed a cube with 250^3 voxels, spatial resolution of 4.10 μm x magnifying factor of 4 (total spatial resolution of 16.40 μm) with estimated value of porosity of 48.20 %. Figure 4 presents the frequency of pores as a function of pore size range for 3D model, which indicates that approximately 57.60% of the material porous phase refers to pores with radius varying from 20.48 to 57.34 μm. The pore size distribution curve of the 3D model reconstructed by truncated Gaussian method does not reproduce pore sizes bigger than 65.5 μm, which were measured in 2D images. The 3D volume with 250^3 voxels is not sufficient to generate big pores. To generate a 3D volume bigger than 250^3 voxels it is necessary to use computers with high image processing performance.

Figure 5a shows the 3D μ-CT image reconstructed with 500 images of the Ti porous sample slices, which achieved a spatial resolution of 2.90 μm. Figure 5b presents a 2D binary section obtained by μ-CT, where Ti is the white phase. The rendered 3D image can be seen as a porous solid and the detail shows the interconnected macroporosity structure.

Figure 6 shows the 3D topographic map of the sample obtained by CSOM. The image, with dimensions of 4.275 mm (height) x 5.637 mm (width) x 660.7 μm (thickness), refers to the primary profile (original image). To determine roughness and waviness of a 2D profile, Fast Fourier Transformation filtering is applied to separate the long-wavy and short-wavy profile components. By filtering a measured profile (primary data, P-profile), a roughness filtered profile (R-profile) and a waviness filtered profile (W-profile) can be obtained[17].

The primary profile parameters of the Ti porous sample were assessed on four different points. Figure 7 illustrates the spectrum of one of the points analyzed. The average height of primary profile (Pa) is 52.11 ± 10.67 μm; the mean peak to valley height of primary profile (Pz) is 325.63 ± 62.09 μm; the maximum peak to valley height of primary profile (Pt) is 395.88 ± 48.88 μm. The roughness profile was also analyzed and the following parameters were obtained: 42.32 ± 5.77 μm (average roughness of roughness profile – Ra); 283.2 ± 32.95 μm (mean peak to valley height of roughness profile - Rz); 392.35 ± 44.53 μm (maximum peak to valley height of roughness profile - Rt).

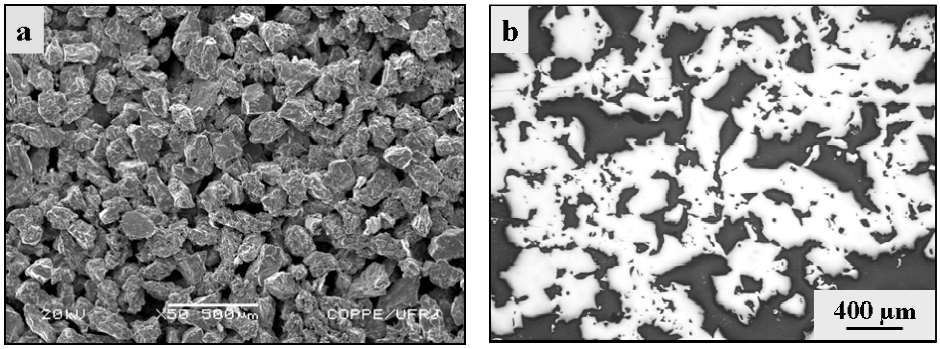

Figure 1. Ti porous sample: SEM topographic view (a); optical micrograph (b).

Table 1. Porosity measurements by geometric method (GM), gamma-ray transmission technique (GRT), quantitative metallographic analysis (QMA) and computed x-ray microtomography (μ-CT).

Sample	Porosity (%)			
	GM	GRT	QMA	μ-CT
85%Ti/15%urea	43.86 ± 2.80	42.92 ± 1.14	47.80 ± 3.00	41.06 ± 0.55

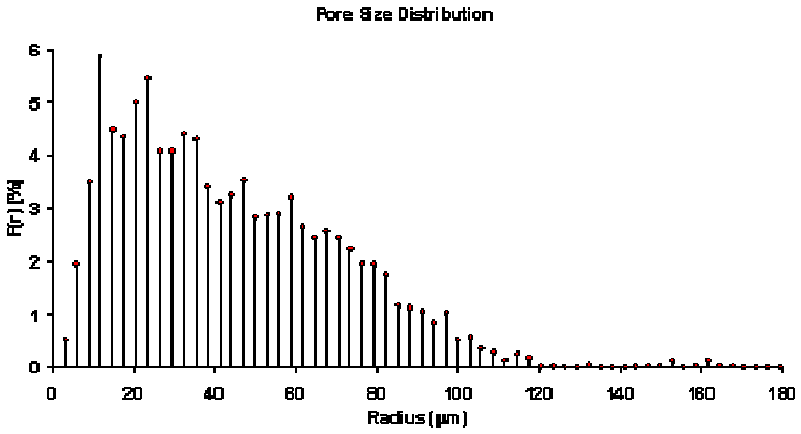

Figure 2. Pore size distribution for 2D image (Figure 1b): frequency of pores x pore radius.

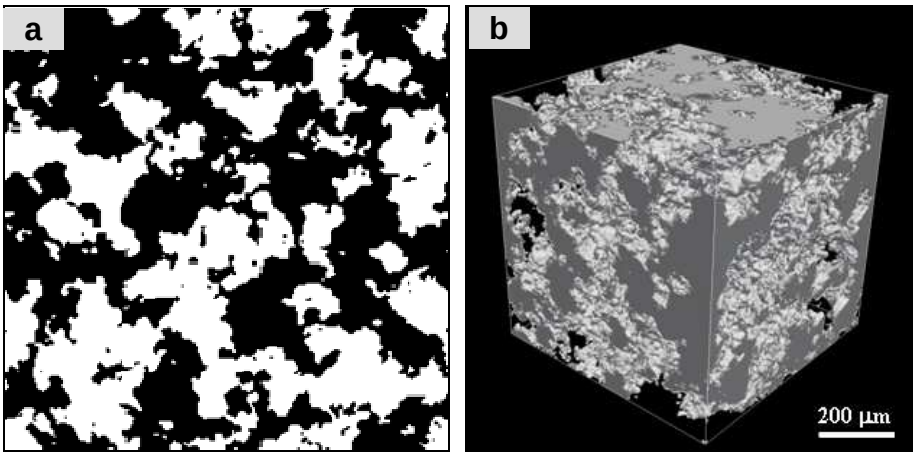

Figure 3. Ti porous sample: 2D binary section generated by the model where pore is the white phase (a) and 3D model generated by truncated Gaussian method (b).

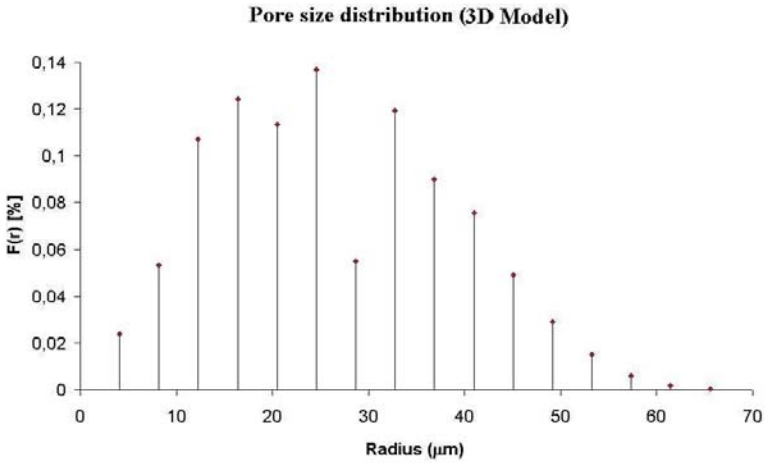

Figure 4. Pore size distribution of 3D model of the porous Ti sample.

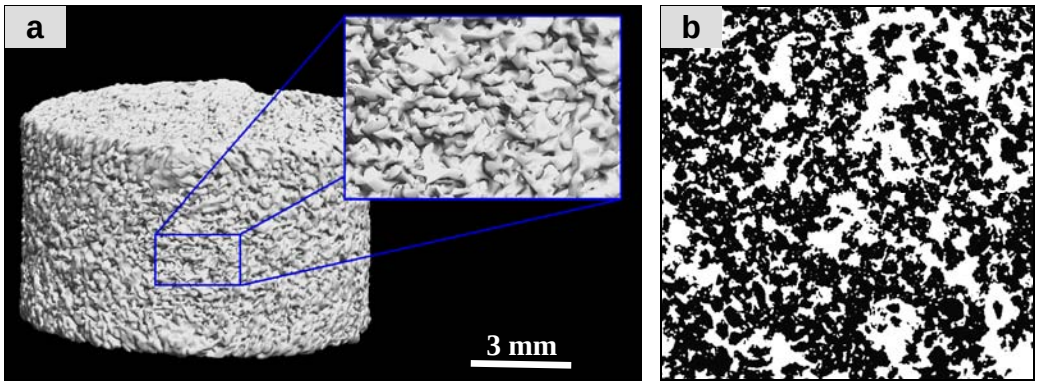

Figure 5. Ti porous sample: 3D µ-CT image (a); 2D binary section by µ-CT where Ti is the white phase (b).

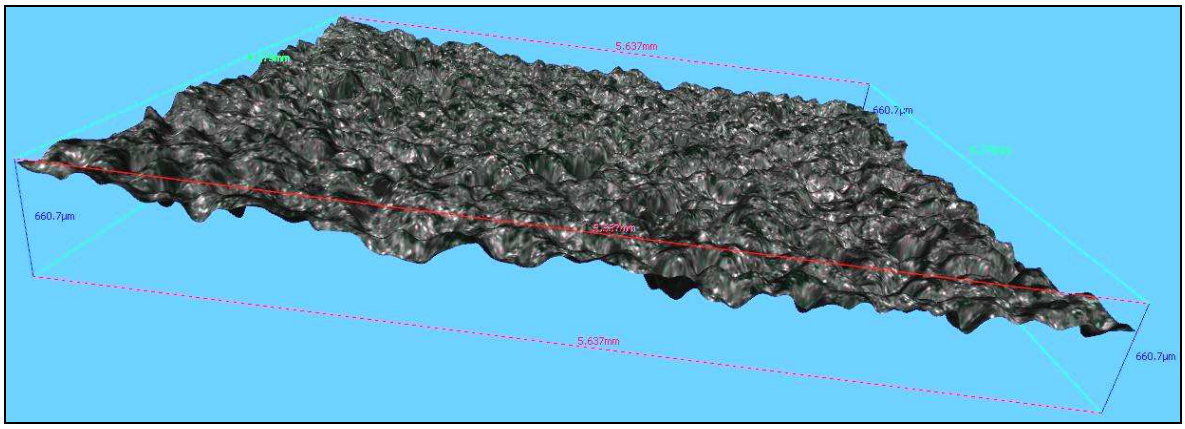

Figure 6. 3D primary profile image of the Ti porous sample obtained by CSOM.

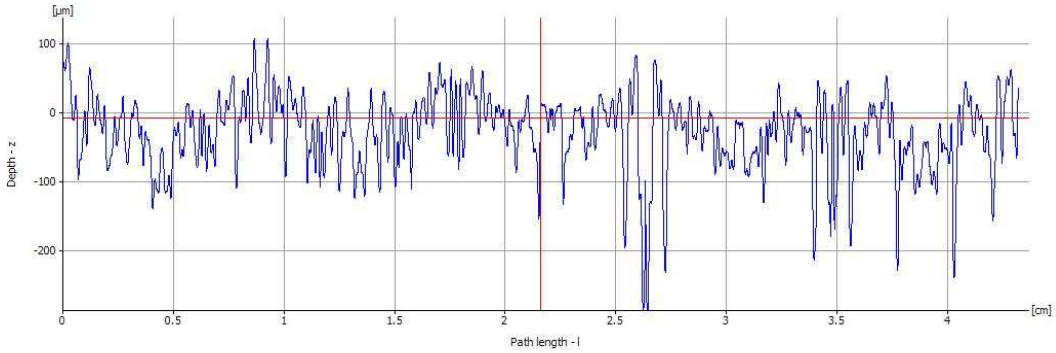

Figure 7. Ti porous sample: spectrum of the primary profile parameters.

In the GM method, the mass measured is the real one but the method considers the volume sample as a dense piece, without pores, inducing errors in the density value. Also this method is quite dependent on human ability.

The GRT technique has many advantages over conventional structural characterization methodologies as it is faster, non-destructive and also does not require sample preparation. By this technique the total porosity of samples can be determined, including closed and open pores.

The QMA method is quite dependent on human ability and the analysis is usually made in only one transverse section of each sample, as sample preparation is time consuming and difficult, specially for soft metals like Ti. Both reasons may induce measurement errors. This method has also the disadvantage of being destructive.

The 3D reconstruction (truncated Gaussian method) is an interesting method since it provides fast and inexpensive results. However, it presents pitfalls when dealing with long-range connectivity, such as in interconnected porous materials with high porosities where only the use of higher order statistics (multiple-point function) can achieve the goal.

Serial sectioning in µ-CT is not often used since it demands the acquisition of hundreds of 2D images of sections for each sample, resulting in a delicate and time

consuming technique. Although µ-CT scanners are not routinely available yet, they grant the acquisition of 2D images with a spatial resolution of a few micrometers that can be rendered as a 3D volume with enough details to characterize the pore structure.

Unlike conventional microscopy, CSOM reconstructs the field measured by *x-y* scanning. The optoelectronic setup, based on a confocal, z-axis extended field, permits a high resolution non-contact 3D surface metrology, including roughness characterization and surface flaw detection.

Further *in vivo* and *in vitro* tests will be performed in the continuity of the research, in order to correlate the material biocompatibility with the porosity data determined by the techniques used in this work.

CONCLUSION

The porous samples processed by powder metallurgy with 15% of pore former presented pore morphology and pore size distribution adequate for surgical use. It also showed a good level of porosity homogeneity which is related to processing reproducibility. However, porosity volume fraction is in the lower level of the range for implant applications. The characterization of a porous media by image analysis is directly influenced by the software operator intervention. The regions analyzed and the noise artifacts presented by the QMA images, besides the illumination gradients, can be responsible for the differences among the porosity values presented by the QMA over the GRT, GM and µ-CT techniques. Among the techniques used in the present work, µ-CT showed to be more suitable for the Ti porous samples evaluation as it is non-destructive and allows to quantify the porosity and the 3D pore size distribution, being more representative to report the porosity quantity and homogeneity. In addition, CSOM showed a powerful technique to create a topographic map and characterize the roughness surface by a non-contact 3D surface metrology.

ACKNOWLEDGEMENTS

The authors thank to “Conselho Nacional de Desenvolvimento Científico e Tecnológico” (CNPq), “Fundação Carlos Chagas Filho de Amparo à Pesquisa do Estado do Rio de Janeiro” (FAPERJ) and Iberoamerican Network BioFab-CYTED for financial support, Rone Felipe da Silva, Elizabete Fátima Nunes, José Luiz de Oliveira and Helga Stefania Maranhão Bodstein for technical assistance.

REFERENCES

1 RYAN, G.; PANDIT, A.; APATSIDIS, D.P. Fabrication methods of porous metals for use in orthopaedic applications. Biomaterials, v. 27, n. 13, p. 2651-2670, May 2006.

2 WEN, C.E.; YAMADA, Y.; SHIMOJIMA, K.; SAKAGUCHI, Y.; CHINO, Y.; HOSOKAWA, H.; MABUCHI, M. Novel titanium foam for bone tissue engineering. Journal of Materials Research, v. 17, n. 10, p. 2633-2639, October 2002.

3 LOPEZ-HEREDIA, M.A.; SOHIER, J.; GAILLARD, C.; QUILLARD, S.; DORGET, M.; LAYROLLE, P. Rapid prototype porous titanium coated with calcium phosphate as a scaffold for bone tissue engineering. Biomaterials, v. 29, n. 17, p. 2608-2615, June 2008.

4 SHEN, H.; OPPENHEIMER, S.M.; DUNAND, D.C.; BRINSON, L.C. Numerical modeling of pore size and distribution in foamed titanium. Mechanics of Materials, v. 38, n. 8-10, p. 933-944, August-October 2006.

5 OLIVEIRA, M.V.; PEREIRA, L.C.; CAIRO, C.A.A. Titanium powder processing with binder addition for medical applications. Materials Science Forum, v. 498-499, p. 173-178, November 2005.

6 KARAGEORGIOU, V.; KAPLAN, D. Porosity of 3D biomaterial scaffolds and osteogenesis. Biomaterials, v. 26, n. 27, p. 5474-5491, September 2005.

7 OH, I.H.; NOMURA, N.; MASAHASHI, N.; HANADA, S. Mechanical properties of porous titanium compacts prepared by powder sintering. Scripta Materialia, v. 49, n. 12, p. 1197-1202, December 2003.

8 LAPTEV, A.; VYAL, O.; BRAM M.; BUCHKREMER, H.P.; STÖVER, D. Green strength of powder compacts provided for production of highly porous titanium parts. Powder Metallurgy, v. 48, n. 4, p. 358-364, December 2005.

9 MOREIRA, A.C.; APPOLONI, C.R.; OLIVEIRA, M.V.; FERNANDES, C.P. Structural characterization of titanium porous foams by gamma rays transmission and x-ray microtomography. International Nuclear Atlantic Conference, Santos, SP, Brazil, September 30 to October 5, 2007.

10 BARUCHEL, J.; BUFFIERE, J-Y.; MAIRE, E.; MERLE. P.; PEIX, G. X-ray tomography in material science. Paris: Hermes Science Publications, 2000.

11 TESEI, L.; CASSELER, F.; DREOSSI, D.; MANCINI, L.; TROMBA, G.; ZANINI, F. Contrast-enhanced X-ray microtomography of the bone structure adjacent to oral implants. Nuclear Instruments and Methods in Physics Research A, v. 548, n. 1-2, p. 257-263, August 2005.

12 GERWARD, L.; GUILBERT, N.; JENSEN, K.B.; LEVRING, H. X-ray absorption in matter. Reengineering XCOM. Radiation Physics and Chemistry, v. 60, n. 1-2, p. 23-24, January 2001.

13 APPOLONI, C.R.; RODRIGUES, C.R.O.; FERNANDES, C.P. X-ray microtomography study of a sandstone reservoir rock. Nuclear Instruments & Methods in Physics Research A, v. 580, n. 1, p. 629-632, September 2007.

14 LIMA, I.; GIRALDES, L.N.; PEREIRA, L.C.; OLIVEIRA, M.V.; LOPES, R.T. Characterization of titanium implant through Micro CT. Nuclear Instruments and Methods in Physics Research A, v. 579, n. 1, p. 309-312, August 2007.

15 YATCHMENOFF, B.; COMPTON, R.D. Ceramic surface analysis using optical sections. American Ceramic Society Bulletin, v. 69, p. 1307-1310, August 1990.

16 LANGE, D.A.; JENNINGS, H.M.; SHAH, S.P. Analysis of surface roughness using confocal microscopy. Journal of Materials Science, v. 28, n. 14, p. 3879-3884, January 1993.

17 CALVIMONTES, A.; GRUNDKE, K.; MÜLLER, A.; STAMM, M. Advances for the topographic characterisation of SMC materials. Materials, v. 2, n. 3, p. 1084-1103, August 2009.